International Journal of Earth Sciences (2026) 115:17
https://doi.org/10.1007/s00531-026-02568-9

ORIGINAL PAPER

Radiolytic CH_4 and CO_2 from irradiated organic compounds

Arndt Schimmelmann[1] · Alex L. Sessions[2] · Aliaksandra Lisouskaya[3] · Anže Jazbec[4] · Simon C. Brassell[1] · Bor Krajnc[4] · Doris Potočnik[4] · Nives Ogrinc[4]

Received: 2 August 2025 / Accepted: 20 February 2026

Abstract
The chemical composition of sedimentary organic matter is often used to reconstruct Earth's biogeochemical history. However, few studies have considered that the long-term effects of subterranean natural radioactivity over geologic time can be common enough and provide sufficient activation energy to trigger radiolysis and the generation of methane, carbon dioxide, and other gases. We performed separate α-, β-, and γ-irradiation experiments at low temperatures on chemically diverse and pure model organic compounds in evacuated and sealed glass tubes to test the hypothesis that radiolytic C–C bond cleavage can result in radiolytic methane and carbon dioxide. α-Irradiation utilized uranium oxide powder mixed with organic model compounds, whereas β- and γ-irradiation experiments relied on β-radiation from ^{90}Sr (370 MBq or 10 mCi) and on delayed γ-ray energy in a TRIGA nuclear research reactor, either 25 kGy typical for biosafety sterilization or 1 MGy. We report initial experimental evidence from ongoing experiments after up to three years of irradiation. Widespread observations of methane in the headspaces of γ-irradiated sealed glass tubes identified radiolytic methanogenesis. Carbon dioxide was observed when organic compounds with carboxyl groups were γ-irradiated. For example, 2.2 % of glycine was converted to methane and carbon dioxide during 1 MGy of γ-irradiation. α-Irradiation produced measurable methane only from squalane which is particularly rich in methyl groups. ^{90}Sr produced insufficiently intense β-irradiation to yield measurable headspace gases. Our study offers an improved organic-molecular understanding of which functional groups and carbon skeletal configurations lend themselves to radiolytic methanogenesis and generation of carbon dioxide.

Keywords Ionizing radiation · Radioactivity · Radiolytic gas · Radiolysis · Methane · Carbon dioxide

Introduction

The genesis of natural gas components methane and carbon dioxide from sedimentary organic matter (SOM) is traditionally framed in terms of biodegradation, oxygen availability, temperature-dependent reaction rates, and sometimes pressure and geo-catalysis. Activation energies needed for the formation of smaller molecules from SOM can also be supplied by ionizing radiation from radioactive decay. Uranium and thorium isotopes and their radioactive progeny along their extended decay series are a primary source of natural, subterranean radiation. Relative enrichment of radioactive uranium is typically observed in organic-rich sediments and rocks. The concentration of total organic carbon (TOC) in black shales is generally proportional to the uranium abundance, averaging 8 ppm by weight, because both TOC and U accumulate syndepositionally (Schmoker 1981) and uranium is diagenetically concentrated in distinct macerals (Liu et al. 2020). The correlation between U and SOM is strong enough that radiation is also used empirically as a borehole logging tool during petroleum exploration (Lüning and Kolonic 2003). Radiation terms and units employed in the following text are explained on an EPA website (EPA 2021).

A short review of relevant, poorly cross-referenced earlier studies is appropriate. There is strong empirical evidence for radiation-based chemical changes in SOM over geologic time (Boreham et al. 2022; Yin et al. 2023). Based on the unusual geochemistry of SOM in the middle Cambrian–Lower Ordovician uranium-rich Alum Shale (Schulz et al. 2021) with intense internal α-radiation (~100 ppm

✉ Arndt Schimmelmann
aschimme@iu.edu

1 Indiana University, Bloomington, IN, USA

2 California Institute of Technology, Pasadena, CA, USA

3 University of Notre Dame, Notre Dame, IN, USA

4 Jožef Stefan Institute, Ljubljana, Slovenia

Published online: 10 March 2026

U; radiation dose of 10^8–10^9 Gy over ~500 Ma), Yang et al. (2018, 2019, 2020) argued that radiation from uranium caused SOM to cross-link and form aromatized and dealkylated (e.g., demethylated) macromolecules, echoing an earlier interpretation of organic compositional data by Dahl et al. (1988a). Dahl et al. (1988b) further observed a general increase in the atomic O/C ratio of Alum Shale SOM with increasing uranium concentration, which was interpreted as radiation-induced oxidation of SOM. Yang et al. (2018, 2020) explain the inverse proportionality between kerogen atomic H/C ratios in Alum Shale SOM and the natural logarithm of the uranium concentration to be a result of progressive dealkylation, aromatization, and cross-linking. Similar conclusions were reached by Jaraula et al. (2015) based on radiolytic alteration of biopolymers in the Mulga Rock uranium deposit in Australia with > 5300 ppm U closely associated with SOM. Dealkylation in particular would result in the liberation of short-chain hydrocarbon radicals that require additional hydrogen to quench. For example, the radiolytic loss of a methyl group can yield methane if a hydrogen atom is either abstracted from organic matter or supplied by water radiolysis (Sauvage et al. 2021)—an important source of reactive hydrogen in geological systems, where water is ubiquitous and most subsurface chemical reactions occur in or near aqueous environments. The radiolytic origin of some hydrocarbons in natural gas has been proposed by Silva et al. (2019) and Naumenko-Dèzes et al. (2022).

Several experimental irradiation studies reporting the generation of gases from SOM face shortcomings in terms of (i) variable presence of water during irradiation, since irradiation of H_2O can open up new reaction pathways involving H atoms and ·OH radicals, which are diffusible and can reach surface-adsorbed organics; (ii) failure to rigorously exclude atmospheric O_2 and thus choosing experimental conditions that are far different from typically anoxic sedimentary environments of organic-rich rocks; irradiation of O_2 can strongly accelerate radical reactions of hydrocarbons; (iii) most studies have focused on high dose rates of β- and γ-radiations, rather than the α particles more common in sedimentary rocks. Experimental β-irradiation of Green River Shale "in an evacuated Pyrex® tube using an electron beam from a linear accelerator" with an absorbed radiation dose of 1 MGy (the scant experimental description leaves open whether the significant attenuation of β-radiation through Pyrex® glass was accounted for) by Dahl et al. (1988b) generated a "wet" hydrocarbon gas mixture (i.e., methane and higher homologous hydrocarbons). Silva et al. (2019) sealed gas-free crude oils under argon in glass ampoules and exposed them to γ-radiation from a ^{60}Co source at a dose rate of 13.05 kGy h^{-1} (Larter et al. 2019), which yielded mixtures of C_1–C_5 hydrocarbon gases. The authors proposed that contributions of radiolytically generated hydrocarbon gases may be significant in some natural gas plays. Lewan et al. (1991) γ-irradiated thermally immature samples of Phosphoria Retort Shale and its isolated kerogen at absorbed radiation doses from 0.81 to 8.85 MGy from a ^{60}Co source. They measured the yields of methane and ethane (along with CO_2, CO, H_2, and N_2) that were produced radiolytically and reported up to 4.7 µmol of methane and 0.6 µmol of ethane per gram of organic carbon in shale or kerogen. Gulieva et al. (2020) applied 200 kGy of γ irradiation from ^{60}Co to waterproofing asphalt and noted the liberation of gases (H_2, CO, CH_4, C_2H_4, C_2H_6, and higher homologues) as well as chemical structural changes. Wang et al. (2022) irradiated immature kerogen and bitumen with γ-rays, and decane was irradiated using an electron beam. The experiments did not rigorously exclude atmospheric oxygen. Ruptures of C–H and R–CH_3 bonds liberated H_2 and CH_4 with concomitant structural alterations of kerogens and bitumen involving cracking, cross-linking, and oxidation reactions. Oxygen-containing group cleavage liberated carbon dioxide. Water radiolysis provided oxygen for the oxidation of organic matter and promoted H_2 generation. Radiolysis decreased H/C and increased O/C elemental ratios. Observed dealkylation, aromatization and unsaturation reactions were similar to thermal effects. The authors concluded that "U irradiation could also promote conventional gas and immature gas generation and could provide exogenous H for hydrocarbon generation of OM, especially for OM in an over mature stage. It is essential to consider the effects of U irradiation on the evolution, hydrocarbon generation, and resources assessment of U-rich shales."

Various kinds of experimental irradiation in combination with numerous types of non-SOM organic substrates were reported to (i) widely liberate hydrogen, methane, ethane, and other short-chain hydrocarbons, (ii) cause hydrogen loss and aromatization, and (iii) lead to complex polycondensation/polymerization. A few representative examples are cited here. Irradiation of pure methane with α particles from radon at 25 °C (or by 100 eV β-radiation) resulted in 7.5 to 18 % conversion and produced mixtures containing H_2, C_2H_6, C_3H_8, and C_4H_{10} (see review by Swallow 1960, p. 62). Absorbed doses of γ-irradiation in the range of 29.7–237.6 kGy liberated gaseous products H_2, CH_4, C_2H_4, and higher homologues from transformer oil (Iskenderova and Kurbanov 2019). γ-Irradiation of up to 200 kGy of vacuum oils liberated H_2 (up to 30 µmol per gram of oil after 100 kGy) and a host of other volatile and oily radiolysis products (Shostenko et al. 2006). γ-Irradiation of mixtures of water and *n*-hexane produced more molecular hydrogen compared to the radiolysis of

Table 1 Pure organic model compounds, their structure, the rationale for their use in irradiation experiments, their mixing ratios with diatomaceous earth or uranium oxide, as well as their commercial sources and purities

Chemical name	Chemical structure	Rationale for selection	Mixing ratios with diatomaceous earth (DE) or uranium oxide (UO)	Source and purity
5α-Cholestane $C_{27}H_{48}$	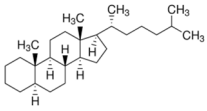	Representative steroidal biomarker, naphthenic component of petroleum	1:1 DE (wt: wt) 1:3 UO (wt: wt)	Sigma-Aldrich #C8003, ≥ 97 wt%
Glycine $C_2H_5ONO_2$	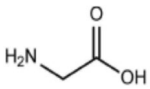	Common amino acid, to study amine and carboxyl chemistry	1:2 DE (wt: wt) 1:3 UO (wt: wt)	USGS65 (Schimmelmann et al. 2016), 99 wt%
n-Icosane (*n*-eicosane) $C_{20}H_{42}$		Similar to plant wax biomarkers, aliphatic (unbranched) component of petroleum	1:1.95 DE (wt: wt) 1:3 UO (wt: wt)	Sigma-Aldrich #44818, 99.8 wt%
Phytol $C_{20}H_{40}O$	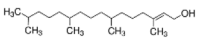	Side chain of chlorophyll *a*, key biomarker for environmental records	1:2 DE (wt: wt) 1:3 UO (wt: wt)	Sigma-Aldrich #W502200, ≥ 97 wt%
Pyrene $C_{16}H_{10}$	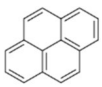	Representative poly-aromatic, aromatic component of petroleum	1:1 DE (wt: wt) 1:3 UO (wt: wt)	Sigma-Aldrich #48570, 98.5 wt%
Squalane $C_{30}H_{62}$	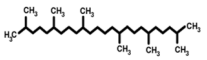	Common biomarker, aliphatic (branched) component of petroleum	1:2 DE (wt: wt) 1:3 UO (wt: wt)	Sigma-Aldrich #234311, 99 wt%
L-Valine $C_5H_{11}NO_2$	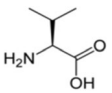	Common amino acid, to study amine and carboxyl chemistry	1:1 DE (wt: wt) 1:3 UO (wt: wt)	USGS73 (Schimmelmann et al. 2016), 99 wt%

water or *n*-hexane alone (Garibov et al. 2004). Direct scaling from relatively short-term laboratory to long-term geological timescales carries uncertainty due to dose rate effects and potential mechanistic differences. While studies of uranium-rich rocks, SOM, oils, and individual hydrocarbons are highly suggestive that natural radiation can and does alter organic matter, they are not well suited to understanding the reaction mechanisms or resulting changes in chemical composition because they are mostly based on complex organic matter, whose starting composition is poorly constrained. The results are also difficult to extrapolate to the lower uranium contents that constitute most of the sedimentary rocks on Earth. Moreover, they confound the effects of different types of ionizing radiation, which are not all equally effective in triggering chemical reactions due to their different energies and linear energy transfer, LET (Burns and Sims 1981; Buxton 2008). γ- and β-radiations are low-LET types with ~0.2–1 keV/µm, while α-radiation has a much higher LET of ~100–150 keV/µm, leading to more localized energy deposition and increased radical recombination. Reductionist laboratory experiments using single model compounds and independently varied radiation doses and types can help us resolve these uncertainties.

Materials and methods

Materials

Seven chemically pure organic model compounds were chosen for irradiation experiments. In contrast to previous studies that irradiated chemically complex sedimentary organic matter (SOM), biological tissue, or food matrix samples, our choice of compounds expresses specific chemical functionalities, reactivities, radiolytic stability, and physical properties (Table 1) representative of those found in natural SOM. 5α-Cholestane, icosane, squalane, phytol, and pyrene are representative of the 4 major classes of hydrocarbon (linear and branched aliphatic, naphthenic, and aromatic) biomarkers studied by biogeochemists and found in petroleum. Glycine and L-valine are included as representative amino acids to study both the chemistry of ionic molecules (i.e., zwitterions in solution at neutral pH) and the amine functional groups. However, we acknowledge that thermal alteration during burial affects the preservation of amino acids and other labile biomarkers in the sedimentary record, effectively precluding their survival as discrete compounds in ancient, mature rocks.

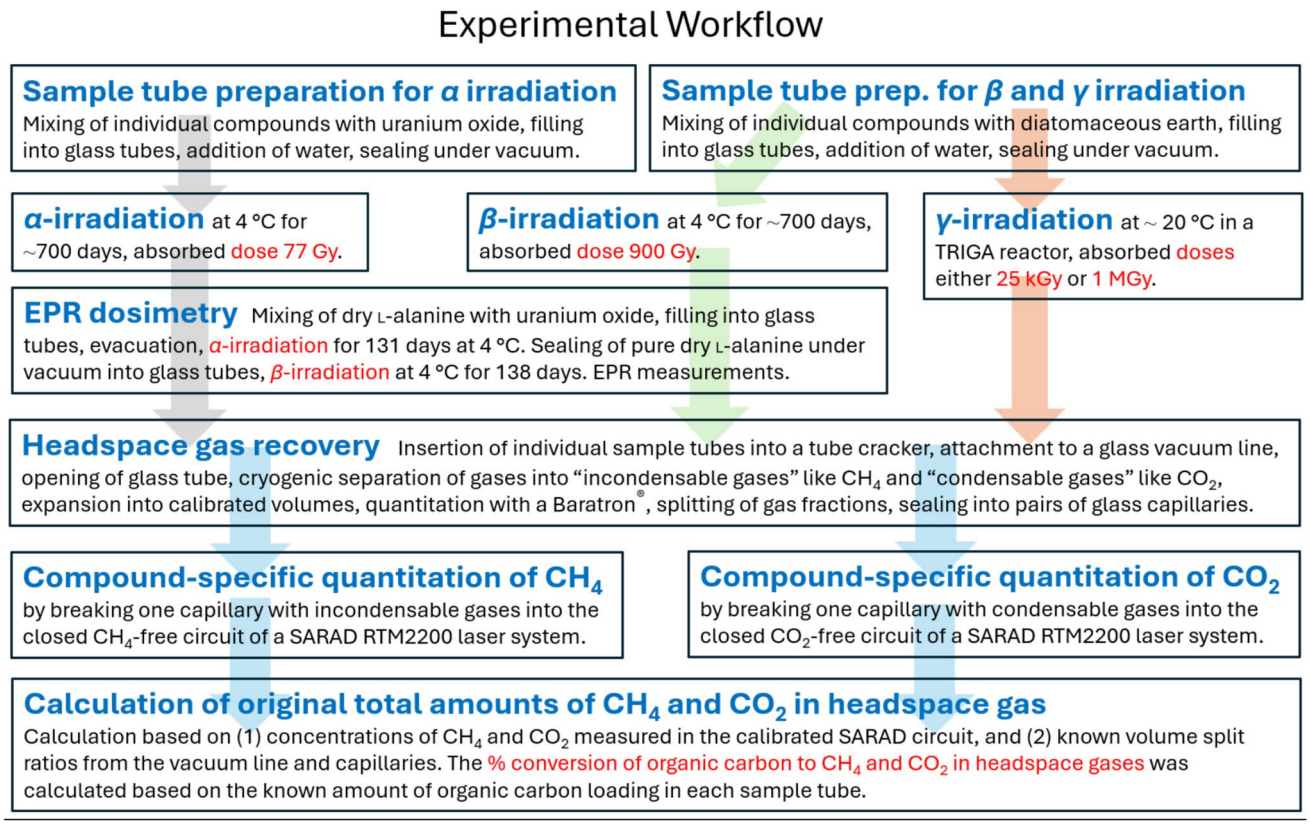

Fig. 1 Overall experimental, analytical, and data processing workflow

Sample loading

The overall workflow is shown in Fig. 1. Each organic model compound was first mixed in an agate mortar with a pestle with either pre-annealed (500 °C) uranium oxide powder in a weight ratio of ~3:1 (uranium oxide:organic sample, w/w, for α-irradiation), or with acid-washed and pre-annealed diatomaceous earth (i.e. opaline SiO_2, for β- and γ-irradiation) to yield powdery and homogeneous substrates. Waxes were slightly warmed to melt them and aid diffusion into the adsorbent, followed by homogenization in a mortar. All resulting powders could be conveniently weighed and loaded into the bottom of pre-annealed Pyrex® glass tubes. The loading of each organic substrate in a Pyrex® tube was 10 or 20 mg. Prior to sealing, between 10 and 50 µL of deionized water (Table 2) was added to simulate moist subterranean geological conditions. Loaded glass tubes were attached to a vacuum line, evacuated (while cryogenically immobilizing volatile components at −80 °C), and sealed under vacuum with a glass-blowing torch. Slightly different sizes of Pyrex® glass tubes were chosen to account for instrumental spatial restrictions during β- and γ-irradiation. α-Irradiation experiments at Indiana University utilized 10-cm long, 6-mm o.d. Pyrex® tubes, whereas β- and γ-irradiation occurred in ~4-cm long, 5-mm o.d. Pyrex® tubing.

Microbial growth during long-term irradiation experiments was a concern although the absence of oxygen in the evacuated glass tubes effectively precludes aerobic microbial activity. Heat sterilization in an autoclave might introduce thermal artifacts that cannot be disentangled from radiation effects. Our irradiation approach uses lower dose rates at low temperatures over months to years to preclude any localized heating that could induce thermally driven reactions and contribute thermogenic natural gas components. This consideration presents a significant limitation of previous experiments (c.f. Yang et al. 2020). Uranium oxide UO_2 is known to inhibit microbial growth (VanEngelen et al. 2011). Evacuated samples were kept refrigerated in the dark throughout α- and β-irradiation and subsequent storage. Samples for γ-irradiation were express-mailed to the Jožef Stefan Institute Reactor Center in Slovenia and promptly received a sterilizing dose of γ-irradiation.

α- and β-irradiation of organic compounds at Indiana University

Loaded and sealed sample tubes for α-irradiation experiments were stored in a 4 °C laboratory refrigerator for 700 days at Indiana University, from December 2021 until November 2023. ^{235}U-depleted uranium oxide powder

Table 2 Amounts of organic compounds used in individual irradiation experiments, as well as carbon dioxide (CO_2) and methane (CH_4) yields from experiments

Organic compound (sample #)	Organic loading (mg); H_2O (µL)	Carbon dioxide yield (µmol)	Conversion of carbon to CO_2 (%)	Methane yield (µmol)	Conversion of carbon to CH_4 (%)	Total conversion of carbon to CO_2 and CH_4 (%)
α-Irradiation *experiments*						
Phytol (#21)	10.2; 10	Not detected	0	Not detected	0	0
Squalane (#1)	10.9; 10	Not detected	0	0.01	0	0
Squalane (#2)	10.6; 10	Not detected	0	0.04	0.01	0.01
L-valine (#90)	9.6; 20	Not detected	0	Not detected	0	0
β-Irradiation *experiments*						
n-Icosane (#61)	12.0; 20	Not detected	0	Not detected	0	0
Phytol (#48)	11.6; 20	< 0.3	< 0.03	< 0.01 (trace)	0	< 0.003
Squalane (#41)	10.5; 20	Not detected	0	Not detected	0	0
γ-Irradiation *experiments*						
5*α*-Cholestane (#101)	21.2; 30	Not detected	0	0.30	0.02	0.02
Glycine (#23)	22.0; 50	14.7	2.51	1.73	0.29	2.80
n-Icosane (#34)	22.5; 30	< 0.1 (trace)	< 0.01	0.13	0.01	< 0.04
Phytol (#50)	21.2; 40	< 0.5	< 0.03	0.64	0.04	< 0.07
Pyrene (#1)	20.0; 30	Not detected	0	0.01	0	0
L-valine (#17)	31.8; 50	10.4	0.77	0.50	0.04	0.80

Gas yields are used to calculate the carbon conversion (in % of total initial organic carbon contained in the organic loading in the second column) from the organic compounds to gas species CO_2 and CH_4. Detection limits for CO_2 and CH_4 are 0.1 and 0.01 µmol, respectively. For two individual measurements, the final compound-specific gas signals *via* laser oscillated between the zero baseline and the accepted detection limits. These data are characterized as "traces" (i.e. values above the detection limit but below quantification, without stated standard deviation or analytical uncertainty). Similarly, CO_2 signals from phytol, albeit clearly detectable, were more noisy than those from amino acids

as the source of *α*-radiation for our experiments retains ~60 % of the radioactivity of natural uranium (McDiarmid 2001). A uranium content of ~88.2 weight % in UO_2 with a density of 10.96 g cm^{-3} will be lowered slightly upon addition of organic compounds. Assuming a mixture with 85 weight % UO_2, the resulting specific *α* activity is 11.5 kBq g^{-1}, approximately 56,000 times larger than in an average black shale. In other words, one year of lab experiment would simulate the accumulated dose of α particles from 56,000 years of natural radiation. The slow decay of depleted uranium produces minuscule amounts of short-lived radioisotopes that contribute negligible doses of *β*- and γ-radiations.

We employed ^{90}Sr as a source of *β*-radiation because: (i) the ^{90}Sr decay cascade to stable ^{90}Zr does not emit either *α*- or *γ*-radiation, and (ii) it produces high-energy (2.3 MeV) *β* particles similar to the U-series decay in rocks. *β*-Irradiation was performed over 700 days in sealed glass tubes positioned next to a commercial, encapsulated ^{90}Sr source (Fig. 2) in a ~4 °C refrigerator in the laboratory of Indiana University's Radiation Safety Officer from December 2021 until November 2023. A ^{90}Sr source of 370 MBq (10 mCi) was deployed at a distance of ~3 cm from a bundle of ~20 sealed samples (Fig. 2).

γ-Irradiation of organic compounds at the Jožef Stefan Institute, Slovenia

A TRIGA nuclear research reactor at the Jožef Stefan Institute provided *γ*-irradiation (Ambrožič et al. 2017) during reactor shut-down state when neutrons emitted from fuel can be neglected, thus avoiding the complication of induced radioactivity *via* neutron activation. During shut-down state, without sustained chain reactions, only so-called delayed *γ*-rays are emitted with an energy range of ca. 0.01 to 7 MeV. The *γ*-ray intensity depends on the preceding operational history of the reactor (i.e., power level and operation time). For example, to achieve a dose of 25 kGy in shut-down state (i.e., without neutron emission), the samples were irradiated for between 1 and 3 nights. The received *γ* doses were calculated using factors determined by a calibrated detector that was positioned in the exact same location as the samples. *γ*-Irradiation was the most energetic of our experiments. Thus, it represents a worst-case scenario for possible localized heating of samples, which we constrain as follows: In the absence of any heat losses, and taking icosane (heat capacity C_p = 2.132 J/gK) as representative of our organic substrates,

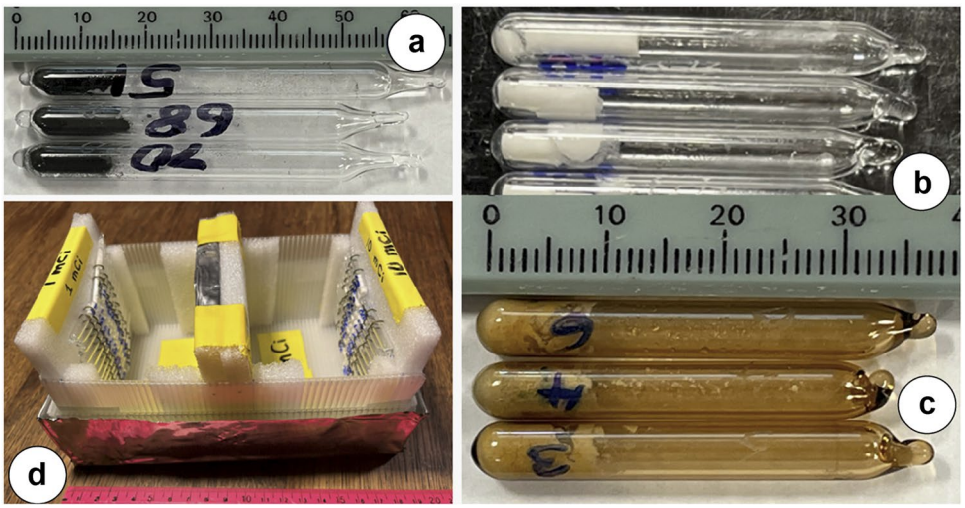

Fig. 2 **a** α-Irradiation experiments in 6-mm o.d. Pyrex® tubes. The dark color derives from uranium oxide; **b** γ-Irradiation experiments in 5-mm o.d. Pyrex® tubes *prior* to irradiation and **c** after 1 MGy γ-irradiation resulting in brown discoloration of the glass. **d** β-Irradiation setup where ^{90}Sr sources are positioned in the center to irradiate numerous sealed Pyrex® glass tubes that are sewn onto foam at a defined distance from the source

an absorbed dose of 25 kGy (= 25,000 J/kg) would lead to a temperature rise of just 11.7 °C. The mass attenuation coefficients for gasoline, water, and glass are all similar for 5 MeV photons, so all absorb γ-rays at roughly the same rate. Pyrex® has the lowest heat capacity (0.75 J/gK) of the three and thus experiences the largest temperature rise (33 °C) of the 3 materials. However, this heating was counteracted by thermal conduction to the surrounding air in the reactor, which was maintained at 20 °C. Thermal conduction through 0.77 mm glass with a representative 10 °C temperature gradient amounts to 13 mW/cm^2 (= 47 J/hr/cm^2). This can be compared to the total energy absorbed per unit area of glass wall (4.4 J/cm^2) to conclude with high confidence that the samples remained within a few degrees of ambient temperature. Radiation damage from γ-rays arises primarily through indirect ionization mechanisms. High-energy photons interact with atoms in the sample *via* processes such as the photoelectric effect, Compton scattering, and at higher energies, pair production. In both the photoelectric and Compton processes, energetic electrons are ejected from atoms, creating secondary electrons that deposit energy locally as they slow down through inelastic collisions. These electrons can break chemical bonds, ionize molecules, and induce structural or chemical changes in the material. As a result, γ-ray exposure can cause molecular degradation, cross-linking, or radiolysis, depending on the sample's composition and the absorbed dose. γ-Irradiation occurred at two cumulative levels of delayed γ-ray energy, either 25 kGy typical for sterilization in biosafety, or 1 MGy. During γ-irradiation in the TRIGA reactor, a short non-intentional neutron irradiation occurred in 2022 amounting to an estimated 26 Gy neutron dose associated with a 14 Gy γ dose. We consider this accidental neutron irradiation negligible in light of the achieved cumulative γ doses of 25 kGy and 1 MGy.

Dosimetry of α- and β-irradiation at the University of Notre Dame

Detailed dosimetry was employed to explain lower gas yields from α- and β-irradiation experiments relative to γ-irradiation. To compare the effects of different types of radiation (α, β, and γ) on organic solids, we performed L-alanine dosimetry to estimate the amount of radicals formed under each radiation exposure. Direct comparisons of absorbed dose across different radiation types are challenging due to their distinct energy deposition mechanisms and penetration depths. L-alanine dosimetry provides a consistent method for quantifying radical yields and thus enables a meaningful comparison of radiation-induced chemical changes. It is important to note that radical yields (G values) in L-alanine dosimetry decrease significantly with increasing linear energy transfer (LET), with the highest yields observed for γ- and β-radiation (G ≈ 0.8–1.0 radicals/100 eV), and substantially lower yields for α-radiation (G ≈ 0.1–0.2 radicals/100 eV) due to enhanced radical recombination within dense ionization tracks. As a result, the radical yields from γ- and β-irradiation can be directly compared, while α-irradiation requires appropriate corrections to account for its higher LET and reduced radical formation efficiency (Hansen et al. 1987).

L-alanine was chosen because its radiation response is representative of many other organic systems. In addition, the mass attenuation coefficients of L-alanine for γ- and β-radiation are similar to those of typical organic solids, especially in the low-to-mid energy range (10 keV to a few MeV; Hubbell and Seltzer 2004).

Both α and β particles can be blocked by glass walls before radiation can interact with the organic target molecules that are sealed in glass tubing. In the case of α-irradiation, this problem was circumvented by directly mixing the α-emitter uranium oxide with the organic compounds, yet the dose could not be calculated from the amount of employed uranium oxide. We applied comparative dosimetry to arrive at the actual α- and β-irradiation doses that were received by organic compounds.

The interaction of ionizing radiation and chemical compounds can generate unpaired electrons that can be quantified by electron paramagnetic resonance (EPR) spectroscopy and serve as a proxy for radiation dose over a wide dose range from 1 Gy to 150 kGy (Regulla and Deffner 1982). EPR measurements of dry L-alanine (SI Science, Japan) were performed at the Radiation Laboratory of the University of Notre Dame to evaluate its response to ionizing α- and β-irradiation for dosimetry purposes (Desrosiers et al. 2008). The response of these L-alanine dosimeters was compared to their response following irradiation with cobalt-60 (^{60}Co) γ-rays. L-alanine samples were irradiated with γ-rays at doses ranging from 38 to 76 Gy using a Shepherd 109-68R irradiator located at the Notre Dame Radiation Laboratory. The dose rate (38 Gy/min) of the irradiator was evaluated using a Fricke chemical dosimeter (Klassen et al. 1999). The dose rate in L-alanine is approximately 97.5 % of that in Fricke solution, based on their mass energy-absorption coefficients for ^{60}Co γ-rays. EPR measurements were carried out using a Bruker EMXplus spectrometer (Bruker Corporation, Billerica, Maryland) equipped with an ER4119HS standard resonator operating in the X-band (9.49 GHz). The following EPR parameters were used: a magnetic field sweep width of 200 G, a sweep time of 30 s, a modulation amplitude of 1 G at a frequency of 100 kHz, and a microwave power of 0.6352 mW. Each spectrum was averaged over 5 scans. The resulting EPR intensity is proportional to the total number of unpaired electron spins in the sample and thus reflects the absolute concentration of paramagnetic species (i.e., radicals).

To quantify the dose from exposure to uranium oxide, which predominantly produces α-radiation, 190 mg of dry L-alanine powder was mixed with 1.7 g of pre-annealed uranium oxide powder resulting in about 10 wt% L-alanine in the mixture, which is similar to weight ratios of mixtures with other organic compounds. The mixture was sealed under vacuum into 6-mm o.d. Pyrex® tubing. The sample was stored in lead foil for 131 days, from January 19th until May 30th, 2025, and then until October 3rd, 2025 for repeat EPR measurements. Dosimetry of β-irradiation relied on 8 additional, dry L-alanine samples (143 to 211 mg) that were sealed under vacuum in multiple 5-mm o.d. Pyrex® glass tubes. Triplets of tubes were exposed at Indiana University to either 37 or 370 MBq (1 or 10 mCi) of β-irradiation from July 31st to December 17th, 2024 (i.e. 138 days) in the same way as other organic compounds had been exposed.

To determine the absorbed dose from the EPR signal, the dosimeter system must first be calibrated with a known radiation field—typically ^{60}Co γ-rays or high-energy electrons, where the dose-to-alanine relationship is well established. The response of the L-alanine dosimeters in our study was compared to their response following irradiation with γ-rays from ^{60}Co. The conversion from signal to dose for α- and β-radiations follows Eq. (1)

$$D_{\mathrm{rad}} = S_{\mathrm{rad}}/k_{\gamma} \cdot f_{\mathrm{rad}} \quad (1)$$

where S_{rad} = EPR signal amplitude (a.u.), D_{rad} = absorbed dose in L-alanine (Gy), k_{γ} = calibration constant obtained with γ-rays ($k_{\gamma} = S_{\gamma}D_{\gamma}$), f_{rad} = correction factor accounting for different radical yields due to LET effects ($f_{\beta} \approx 1.0$ (similar yield to γ-rays); $f_{\alpha} \approx 0.6$–0.8, depending on particle energy and stopping power).

The measured EPR signals represented by 4 differently colored central lines for L-alanine in Fig. 3 are explained as follows: (i) The dark blue line (peak #2) corresponds to $S_{\gamma} = 0.51$ (arbitrary unit, a.u.) with a known absorbed dose of γ-irradiation of 10 wt. % L-alanine in uranium oxide delivered during calibration of $D_{\gamma} = 76$ Gy. The calculated calibration constant (sensitivity) is $k_{\gamma} = S_{\gamma}/D_{\gamma} = 0.51/76 = 0.0067$ a.u./Gy (i.e., a 1-Gy absorbed dose produces 0.0067 a.u. of EPR signal under this calibration). (ii) The red line reflects the measured signal after 37 MBq (1 mCi) of β-irradiation (Fig. 3, red, peak #2) corresponding to $S_{\beta} = 0.72$ a.u. with a relative efficiency for β of $f_{\beta} = 1.0$ ($\beta \approx \gamma$ in L-alanine yield) and a calculated dose of $D_{\beta} = S_{\beta}/k_{\gamma} \cdot f_{\beta} = 0.72/(0.0067 \cdot 1) = 107.5$ Gy. (iii) The green line represents the measured EPR signal after γ-irradiation (Fig. 3, peak #2) with $S_{\gamma} = 0.22$ a.u. and a known absorbed dose delivered during calibration of $D_{\gamma} = 36$ Gy and a calculated calibration constant of $k_{\gamma} = S_{\gamma}/D_{\gamma} = 0.22/36 = 0.0061$ a.u./Gy. (i.e., a 1-Gy absorbed dose produces 0.0061 a.u. of EPR signal under this calibration). (iv) The light blue line shows the measured signal after α-irradiation (Fig. 3, peak #2) corresponding to $S_{\alpha} = 0.17$ a.u. For example, the relative efficiency for α-irradiation is $f_{\alpha} = 0.70$ with reduced radical yield due to high LET and a calculated dose of $D_{\alpha} = S_{\alpha}/k_{\gamma} \cdot f_{\alpha} = 0.17/(0.0061 \cdot 0.7) = 19.5$ Gy.

The comparative EPR measurements of the exposed and formerly blank L-alanine samples indicated specific irradiation doses resulting from the relatively short-term exposures over 131 and 138 days (i.e. ~14.4 Gy of predominantly α-radiation over 131 days, and ~100 Gy at 37 MBq (1 mCi) and ~180 Gy at 370 MBq (10 mCi), respectively, over 138 days of β-irradiation). These doses need to be extrapolated to the ~5 times longer α- and β-irradiation of model compounds at Indiana University

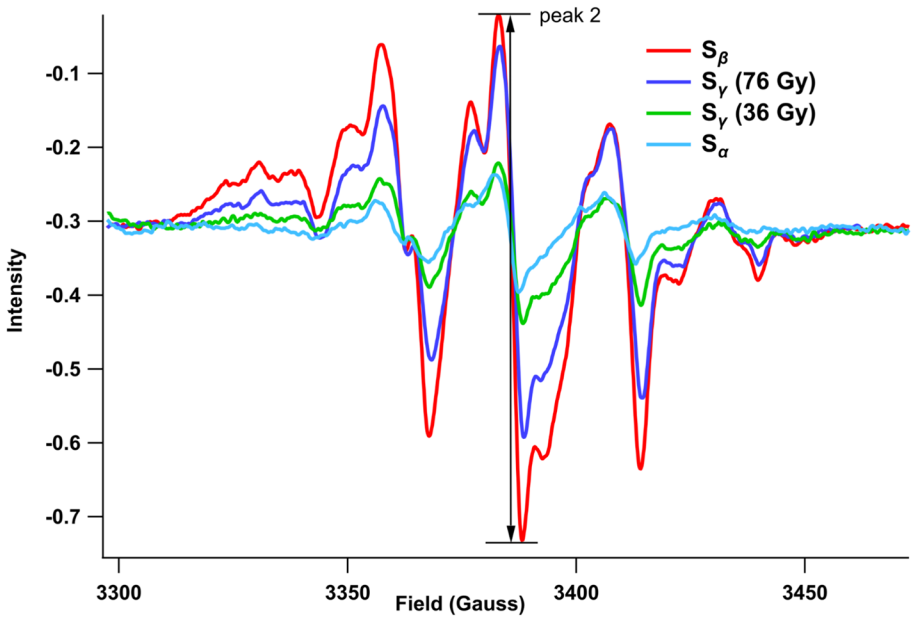

Fig. 3 EPR spectra of radicals formed in L-alanine samples after exposure to irradiation with γ-rays at the University of Notre Dame (S_γ absorbed doses: green 36 Gy measured on October 3rd, 2025, and dark blue 76 Gy measured on January 14th, 2025), β-irradiation (S_β, red), and α-irradiation (S_α, light blue). The intensity is expressed in arbitrary units.

from December 2021 until November 2023. The estimated absorbed doses over ~700 days of α- and β-irradiation of model compounds are ~77 Gy for α-irradiation, and ~900 Gy for β-irradiation at 370 MBq (10 mCi).

Recovery and quantification of radiolytic gases from headspace at Indiana University

Following irradiation, individual glass sample tubes were inserted into a glass cracker assembly that was attached to a dedicated vacuum line to extract non-condensable gases (e.g., H_2, N_2, and CH_4), and condensable gases (e.g., C_2–C_4 hydrocarbons and CO_2) from the headspace, cryogenically trap water, quantify the gas yields in calibrated volumes, and collect splits of the fractions in sealed glass capillaries for subsequent compositional measurements (see methodology and Fig. 1 in Ma et al. 2021). Methane cannot be quantitatively trapped at the temperature of liquid nitrogen without an adsorbent. A 'cold finger appendix' of the vacuum line and the capillaries contain grains of pre-outgassed (*in vacuo* at ca. 450 °C with a yellow flame from a methane-burning torch) coconut charcoal for quantitative collection of methane. Gas yields of bulk condensable and bulk non-condensable gases were determined with a Baratron® pressure gauge in calibrated volumes. Compound-specific methane and carbon dioxide yields were subsequently determined *via* lasers in a SARAD RTM2200 gas detector system (see methodology and Fig. 2 in Ma et al. 2021).

Results

Yields of CH_4 and CO_2 in headspaces as well as the conversion of carbon from irradiated compounds to CH_4 and CO_2 in percent are listed in Table 2. Low yields without clearly discernible traces are indicated as zero. Here we present preliminary results from only 13 individual experiments out of a total of 212 experiments, most of which are still undergoing α-irradiation as of December 2025. CH_4 and CO_2 gas yields above a threshold of 0.01 µmol are additionally plotted logarithmically on Fig. 4.

From the four compounds without organic oxygen (i.e. 5α-cholestane, *n*-icosane, pyrene, and squalane), only γ-irradiation of *n*-icosane generated traces of CO_2, although oxygen was present in all sample tubes in the form of added water that generated ·OH radicals. All significant, quantifiable yields of CO_2 were associated with γ-irradiation of oxygen-containing organic compounds, especially amino acids that can decarboxylate. Glycine was especially prone to radiation-induced decarboxylation and methanogenesis, resulting in 2.8 % of its carbon being converted to CH_4 and CO_2.

Discussion

The radiolysis of solid organic compounds mainly involves ionization (Eq. 2) and excitation (Eq. 3), producing radical cations ($RH^+\bullet$) and excited molecules (RH*) (Mozumder 1999). The chemical effects arise from how the excited or ionized molecules behave—often fragmenting,

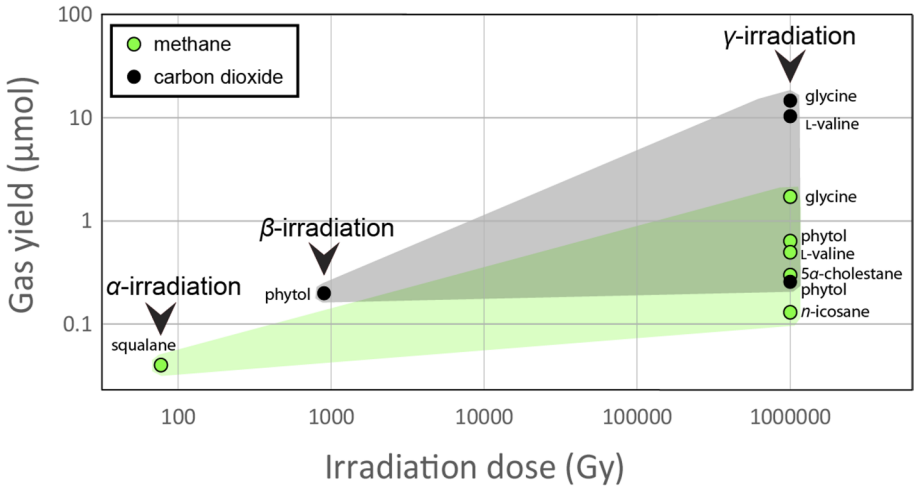

Fig. 4 Methane and carbon dioxide gas yields above a threshold of 0.01 µmol from irradiation experiments. Both axes are logarithmic. Green shading for methane and gray shading for carbon dioxide guide the eye.

rearranging, or polymerizing depending on their structure and energy distribution. In a solid-state environment, radical movement is limited, with C–H bond rupture releasing hydrogen atoms as the most likely process (Eq. 4) that subsequently forms molecular hydrogen (H_2) by abstracting another hydrogen from the initial molecule (Eq. 5) or by recombination of H• atoms (Voevodskii and Molin 1962).

$$\mathrm{RH} \rightsquigarrow \mathrm{RH} + \cdot + \mathrm{e}- \quad (2)$$

$$\mathrm{RH} \rightsquigarrow \mathrm{RH}^{*} \quad (3)$$

$$\mathrm{RH}^{*} \rightarrow \mathrm{R} \cdot + \mathrm{H} \cdot \quad (4)$$

$$\mathrm{H} \cdot + \mathrm{RH} \rightarrow \mathrm{R} \cdot + \mathrm{H}_2 \quad (5)$$

The type and LET of radiation play a critical role in determining the chemical effects and product yields in irradiated organic solids. γ-Rays, with low LET, produce sparse ionizations, leading to moderate product yields due to limited radical migration. α and β particles, with high LET, deposit energy densely within a short range, causing localized ionization, high radical recombination, and structural changes in the surrounding organic matrix. When adsorbed water is present in the solid organic material, the radiation chemistry becomes more complex. Radiolysis of water generates reactive species such as hydroxyl radicals (•OH), hydrogen atoms (H), and hydrated electrons (e^-_{aq}), which can diffuse and react with the surrounding organic matter. This enhances molecular degradation pathways such as oxidation, hydrogen abstraction, and radical-driven bond cleavage. Thus, even in otherwise diffusion-limited solid environments, the presence of water enables additional radiation-induced pathways, altering both the type and amount of products formed.

The types of radiolysis products formed depend on the molecular structure of the organic compound (Collinson and Swallow 1956). Use of a variety of pure compounds with different structures and discrete functional groups rather than complex organics such as SOM enabled us to discern underlying chemical mechanisms for the radiolytic generation of methane and carbon dioxide. Methane can be radiolytically produced by first splitting a methyl radical $\bullet CH_3$ from the organic parent molecule and then supplying a hydrogen atom from either organic matter or water. This pathway explains the absence of methane from pyrene where the condensed aromatic ring structure is devoid of methyl groups (Table 1). Squalane with its 7 methyl groups produced measurable amounts of methane even under comparatively weak α-irradiation, and phytol with 5 methyl groups produced traces of methane as a result of very weak β-irradiation. Among the six γ-irradiated compounds, pyrene with no methyl groups produced the least amount of methane, *n*-icosane with only two methyl groups produced slightly more, and 5α-cholestane (5 methyl groups) and phytol (5-methyl groups) generated progressively more methane. Amino acids are exceptions because their zwitterion character promotes decarboxylation and deamination, which generates radicals that can subsequently react with other molecules to produce methane. This explains that L-valine with only two methyl groups and even glycine, which has none, can generate substantial amounts of methane.

Carbon dioxide was either absent or present only in trace or small amounts after irradiation of compounds that had no oxygen in their molecular structure (i.e., 5α-cholestane, *n*-icosane, pyrene, squalane), regardless of the type of radiation. In contrast, carbon dioxide was an abundant and even predominant radiolytic product in the headspace after γ-irradiation of carboxyl-bearing amino acids. The presence

of oxygen in hydroxy groups in the organic parent molecule was apparently a precondition for the generation of carbon dioxide from phytol. It seems that the availability of •OH radicals from radiolysis of water was insufficient to generate significant amounts of carbon dioxide from organic molecules without oxygenated functional groups (Garrett et al. 2005). The most carbon dioxide was generated from γ-irradiated amino acids glycine and L-valine, which produced carbon dioxide from 2.51 and 0.77 % of their initial organic carbon pools, respectively (Table 2). This aligns with known behaviors in aqueous solution, where amino acids primarily undergo deamination and decarboxylation under radiation. While deamination is known to proceed *via* oxidation and reduction pathways, radiation-induced decarboxylation is less well understood (e.g., Bonifačić et al. 1998). Our measured CO_2 yields are likely an underestimate because concurrent deamination of glycine and L-valine generated ammonia that reacted with CO_2 and H_2O to form non-volatile (solid or dissolved) ammonium carbonate $(NH_4)_2CO_3$ and reduced the amount of free CO_2 in headspace gas. Our results compare well with earlier observations. For example, Cherubini and Ursini (2015) reported that decarboxylation and deamination products were detected using mass spectrometry after pure L-valine had been sealed under vacuum in glass tubes and was γ-irradiated at a dose rate of 0.8 kGy/h for a total dose of 3.2 MGy. Almost 30 % of the irradiated L-valine had reacted during irradiation, and some products resulted from L-valine reacting with CO_2. Carbon dioxide was also observed as an unexpected major gas product from low-temperature γ-irradiation experiments of Phosphoria Retort Shale and its isolated kerogen (Lewan et al. 1991).

Our observation of radiation-induced decarboxylation of organic matter has biogeochemical relevance for interpreting the limited abundance of carboxyl groups in SOM. The composition of carboxylic acids in the sedimentary record is governed by many constraints and competing processes of generation, alteration, and degradation, which include: (1) Most carboxyl groups present in SOM originate from biosynthetic fatty acids and amino acids, together with humic substances formed naturally in aquatic environments (Orem et al. 1986). Attributing the loss of some carboxyl groups in SOM to long-term natural radiation must acknowledge that their microbial accessibility in immature sediments fosters their degradation and incorporation into kerogen. In addition, 'free' fatty acids are more prone to degradation than 'bound' fatty acids that are physically shielded or occluded within organic matter (Kawamura and Ishiwatari 1985), which plays into the balance between preservation and degradation (Ravin et al. 2017). Even 'bound' fatty acids are exposed to the effects of long-term natural radiation in sediments, with an undiminished propensity to undergo decarboxylation. (2) A variety of natural processes generate carboxylic acids by oxidation of biolipid precursors, which can occur during transport and deposition, during sediment diagenesis, or by microbial alteration of petroleum. For example, carboxylic acids are generated from plant wax alkanes by oxidation during eolian transport and are prominent in aerosols (Anttila et al. 2005) and can be formed during diagenetic alteration of SOM, such as the generation of hopanoic acids from bacterial hopanepolyols (Saito and Suzuki 2007). Microbial processes associated with petroleum biodegradation also generate organic acids from hydrocarbon precursors (Meredith et al. 2000). (3) Several non-radiative pathways involve decarboxylation processes during diagenetic alteration, including the conversion of diterpenoid acids to diterpenoid hydrocarbons (Murae et al. 1996). Decarboxylation of kerogens also occurs at higher thermal maturity (Ashida et al. 2005). (4) The tendency for the concentration of carboxylic acids to decrease relative to hydrocarbons during sediment burial can be attributed to the effects of progressive diagenesis and the increasing maturity of SOM, as illustrated by results from marine sediment sequences (Ravin et al. 2017) although acids can survive in immature shales (Barnes et al. 1979; Vandegrift et al. 1980) prior to de-functionalization (Farrimond et al. 2002). The accepted paradigm is that the presence of a carboxyl group facilitates microbial degradation of SOM, perhaps because of solubility considerations. (5) The emphasis on examination of hydrocarbons in more mature rocks means that the persistence of carboxylic acids with increasing thermal maturity is poorly constrained, in part because of concerns for contamination. Recognition of carboxylic acids in ancient rocks in the 1960s (Abelson et al. 1962) is now suspected to represent non-indigenous compounds, a concern that has prompted meticulous care in assessing the potential for contamination from younger strata and mobile hydrocarbons (Hallman et al. 2011; French et al. 2015). Available radiolytic energy from the decay of radioactive isotopes has varied throughout Earth's history (Karam and Leslie 2005). Hence, the importance of radiolytic overprinting was greater in the past, likely peaking about ~2.5 Ga at the end of the Archaean, potentially significant for providing substrates suitable for utilization by bacteria and Archaea. Hence, the importance of radiolytic overprinting was greater in the past, likely peaking about ~2.5 Ga at the end of the Archaean, as illustrated by the natural fission reactor at Oklo, Gabon (Jensen and Ewing 2001). This energy was potentially significant for providing substrates suitable for utilization by bacteria and Archaea in early Earth history. In addition, organic materials delivered to the Earth from space, which was a prevalent source of organic matter during the Archean (Martins and Pasek 2024), experience exposure to cosmic radiation from X-rays and γ-irradiation.

At the onset of our multi-year irradiation experiments, we underestimated the attenuation of β-irradiation from ^{90}Sr when passing through a thin layer of borosilicate glass that

rendered our β-irradiation setup suboptimal due to glass shielding. The unexpectedly low-dose delivery is likely responsible for low gas yields rather than due to intrinsic inefficiency of β-irradiation. The β-irradiation dose rate was insufficient to allow firm conclusions. The same complication was avoided for α-irradiation by directly mixing ^{235}U-depleted uranium oxide powder with organics, yet we discovered that even 700 days of irradiation were insufficient to confidently quantify headspace gases. We roughly estimate that the concentration of uranium in direct contact with organic matter in our sample tubes is approximately 56,000 times greater than in an average black shale with ca. 8 ppm by weight uranium. In other words, one year of lab experiment simulates the accumulated dose of α particles from 56 kyr of natural radiation. We still have dozens of parallel α-irradiation experiments running in sealed glass tubes in a refrigerator at Indiana University and hope to make more measurements in the future. As a side note, many of the added waters in our experiments had used heavy water (^2H_2O, deuterium oxide) and a future compound-specific study on the original and the irradiated organic compounds will be expected to yield valuable insight about radiation-induced hydrogen stable isotope exchange between hydrogen in organics and that in water in contact with SOM. With a low natural abundance of deuterium (^{2}H) in total hydrogen on Earth of approximately 0.016 % and our analytical precision being able to detect differences of only 1 permil, even a small transfer of water-derived ^{2}H into organic hydrogen should be detectable. Future experiments will vary the presence of water and will thus more systematically explore water's role in radiolysis.

Our results are relevant for (i) long-term biogeochemical transformations of fossil organic matter and the likely radiolytic generation of hydrocarbons, (ii) radioecology of subterranean life (e.g., in the deep biosphere) and in contaminated areas, (iii) chemical changes affecting organics in nuclear depositories, (iv) the susceptibility of various types of organic compounds to elevated ionizing radiation on Mars and in space.

Conclusions

(1) ~77 Gy of α-irradiation produced no measurable carbon dioxide and only little methane.
(2) ~900 Gy of β particles were least effective in our experiments to cause methanogenesis (or generation of CO_2) owing to shielding of beta particles by the 5-mm o.d. glass tubes.
(3) γ-irradiation of only 25 kGy did not generate any measurable radiolytic gases. γ-Irradiation of 1 MGy routinely generated measurable quantities of radiolytic methane and in most cases carbon dioxide.
(4) Only compounds with carboxyl groups generated abundant CO_2 upon γ-irradiation. Decarboxylation *via* irradiation may be a contributing factor for low abundances of carboxyl groups in old sedimentary organic matter.

Acknowledgments We gratefully acknowledge the technical support and advice from the Indiana University Radiation Safety Officers Mandi Lynn McKeen and Greg Crouch. Partial financial support was received from the Slovenian Research and Innovation Agency under program P1-0143. EPR experiments at the Notre Dame Radiation Laboratory were supported by the U.S. Department of Energy, Office of Science, Office of Basic Energy Sciences under award number DE-FC02-04ER15533. This is document number NDRL-5480 from the Notre Dame Radiation Laboratory. The authors have no financial or proprietary interests in any material discussed in this article.

Funding The funding was provided by the Slovenian Research and Innovation Agency, program P1-0143 and Office of Science, Award No.: DE-FC02-04ER15533.

Declarations

Competing interests The authors have no competing interests to declare that are relevant to the content of this article.

References

Abelson PH, Hoering TC, Parker PL (1962) Fatty acids in sedimentary rocks. Adv Org Geochem 1962:169–174. https://doi.org/10.1016/B978-0-08-010272-6.50021-5

Ambrožič K, Žerovnik G, Snoj L (2017) Computational analysis of the dose rates at JSI TRIGA reactor irradiation facilities. Appl Radiat Isot 130:140–152. https://doi.org/10.1016/j.apradiso.2017.09.022

Anttila P, Hyötyläinen T, Heikkilä JM, Finell J, Kulmala M, Riekkola M-L (2005) Determination of organic acids in aerosol particles from a coniferous forest by liquid chromatography-mass spectrometry. J Sep Sci 28:337–346. https://doi.org/10.1002/jssc.200401931

Ashida R, Painter P, Larsen JW (2005) Kerogen chemistry 4. Thermal decarboxylation of kerogens. Energy Fuels 19:1954–1961. https://doi.org/10.1021/ef0501086

Barnes PJ, Brassell SC, Comet P, Eglinton G, McEvoy J, Maxwell JR, Wardroper AMK, Volkman JK (1979) Preliminary lipid analysis of core sections 18, 24 and 30 from Hole 402A. DSDP Init Reps 48:965–976. http://deepseadrilling.org/48/volume/dsdp48_50.pdf

Bonifačić M, Štefanić I, Hug GL, Armstrong DA, Asmus KD (1998) Glycine decarboxylation: the free radical mechanism. J Am Chem Soc 120:9930–9940. https://doi.org/10.1021/ja9815428

Boreham CJ, Jinadasa N, Sohn J, Hong Z, Blake C (2022) Characterisation of radiogenic monoalkenes in Australian oils and condensate. Org Geochem 163:104332. https://doi.org/10.1016/j.orggeochem.2021.104332

Burns WG, Sims HE (1981) Effect of radiation type in water radiolysis. J Chem Soc Faraday Trans 1(77):2803–2813. https://doi.org/10.1039/F19817702803

Buxton GV (2008) An overview of the radiation chemistry of liquids. In: Spotheim-Maurizot M, Mostafavi M, Douki T, Belloni J (eds) Radiation chemistry: from basics to applications in material and life sciences, EDP Sciences, pp 3–16. https://doi.org/10.1051/978-2-7598-0317-0.c004

Cherubini C, Ursini O (2015) Amino acids chemical stability submitted to solid state irradiation: the case study of leucine, isoleucine and valine. Springerplus 4:541. https://doi.org/10.1186/s40064-015-1332-9

Collinson E, Swallow AJ (1956) The radiation chemistry of organic substances. Chem Rev 56:471–568

Dahl J, Hallberg R, Kaplan IR (1988a) Effects of irradiation from uranium decay on extractable organic matter in the Alum Shales of Sweden. Org Geochem 12:559–571. https://doi.org/10.1016/0146-6380(88)90147-7

Dahl J, Hallberg R, Kaplan IR (1988b) The effects of radioactive decay of uranium on elemental and isotopic ratios of Alum Shale kerogen. Appl Geochem 3:583–589. https://doi.org/10.1016/0883-2927(88)90090-X

Desrosiers MF, Puhl JM, Cooper SL (2008) An absorbed-dose/dose-rate dependence for the alanine-EPR dosimetry system and its implications in high-dose ionizing radiation metrology. J Res Natl Inst Stand Technol 113:79–95. https://doi.org/10.6028/jres.113.007

EPA, Environmental Protection Agency (2021) https://www.epa.gov/radiation/radiation-terms-and-units (website accessed November 4th, 2025)

Farrimond P, Griffiths T, Evdokiadis E (2002) Hopanoic acids in Mesozoic sedimentary rocks: their origin and relationship with hopanes. Org Geochem 33:965–977. https://doi.org/10.1016/S0146-6380(02)00059-1

French KL, Hallman C, Hope JM, Schoon PL, Zumberge JA, Hoshino Y, Peters CA, George SC, Love GD, Brocks JJ, Buick R, Summons RE (2015) Reappraisal of hydrocarbon biomarkers in Archean rocks. Proc Natl Acad Sci USA 112:5915–5920. https://doi.org/10.1073/pnas.1419563112

Garibov AA, Eyubov KT, Agaev TN (2004) Liquid-phase radiolysis of the water–*n*-hexane system. High Energy Chem 38:295–297. https://doi.org/10.1023/B:HIEC.0000041339.15341.12

Garrett BC, Dixon DA, Camaioni DM, Chipman DM, Johnson MA, Jonah CD, Kimmel GA, Miller JH, Rescigno TN, Rossky PJ, Xantheas SS, Colson SD, Laufer AH, Ray D, Barbara PF, Bartels DM, Becker KH, Bowen JKH, Bradforth SE, Carmichael I, Coe JV, Corrales LR, Cowin JP, Dupuis M, Eisenthal KB, Franz JA, Gutowski MS, Jordan KD, Kay BD, Laverne JA, Lymar SV, Madey TE, McCurdy CW, Meisel D, Mukamel S, Nilsson AR, Orlando TM, Petrik NG, Pimblott SM, Rustad JR, Schenter GK, Singer SJ, Tokmakoff A, Wang LS, Wettig C, Zwier TS (2005) Role of water in electron-initiated processes and radical chemistry: issues and scientific advances. Chem Rev 105:355–390. https://doi.org/10.1021/cr030453x

Gulieva NK, Gatamkhanova GM, Mustafaev II (2020) Radiation resistance of bituminous waterproofing materials. High Energy Chem 54:336–341. https://doi.org/10.1134/S0018143920050057

Hallmann C, Kelly AE, Gupta SN, Summons RE (2011) Reconstructing deep-time biology with molecular fossils. Top Geobiol 36:355–401. https://doi.org/10.1007/978-94-007-0680-4_14

Hansen JW, Olsen KJ, Wille M (1987) The alanine radiation detector for high and low-LET dosimetry. Radiat Prot Dosim 19:43–47. https://doi.org/10.1093/oxfordjournals.rpd.a079918

Hubbell JH, Seltzer SM (2004) X-ray mass attenuation coefficients. NIST standard reference database 126. https://physics.nist.gov/PhysRefData/XrayMassCoef/ComTab/fricke.html

Iskenderova ZI, Kurbanov MA (2019) Changes in performance characteristics of transformer oil by the action of ionizing radiation. High Energy Chem 53:454–458. https://doi.org/10.1134/S0018143919060080

Jaraula CMB, Schwark L, Moreau X, Pickel W, Bagas L, Grice K (2015) Radiolytic alteration of biopolymers in the Mulga Rock (Australia) uranium deposit. Appl Geochem 52:97–108. https://doi.org/10.1016/j.apgeochem.2014.11.012

Jensen KA, Ewing RC (2001) The Okélobondo natural fission reactor, southeast Gabon: geology, mineralogy, and retardation of nuclear-reaction products. GSA Bull 113:32–62. https://doi.org/10.1130/0016-7606(2001)113%3c0032:TOLNFR%3e2.0.CO;2

Karam PA, Leslie SA (2005) Changes in terrestrial natural radiation levels over the history of life. Radiat Environ Biophys 7:107–117. https://doi.org/10.1016/S1569-4860(04)07011-1

Kawamura K, Ishiwatari R (1985) Conversion of sedimentary fatty acids from extractable (unbound + bound) to tightly bound form during mild heating. Org Geochem 8:197–201. https://doi.org/10.1016/0146-6380(85)90026-9

Klassen NV, Shortt KR, Seuntjens J, Ross CK (1999) Fricke dosimetry: the difference between $G(Fe^{3+})$ for ^{60}Co-rays and high-energy x-rays. Phys Med Biol 44:1609–1624. https://doi.org/10.1088/0031-9155/44/7/303

Larter S, Silva RC, Marcano N, Snowdon LR, Villarreal-Barajas E, Sonei R, Paredes Gutiérrez LC, Huang H, Stopford A, Oldenburg TBP, Zhao J, Weerawardhena P, Nightingale M, Mayer B, Pedersen JH, di Primio R (2019) The dating of petroleum fluid residence time in subsurface reservoirs. Part 1: a radiolysis-based geochemical toolbox. Geochim Cosmochim Acta 261:305–326. https://doi.org/10.1016/j.gca.2019.07.020

Lewan MD, Ulmishek GF, Harrison W, Schreiner F (1991) Gamma ^{60}Co-irradiation of organic matter in the Phosphoria Retort Shale. Geochim Cosmochim Acta 55:1051–1063. https://doi.org/10.1016/0016-7037(91)90163-Y

Liu B, Mastalerz M, Schieber J, Teng J (2020) Association of uranium with macerals in marine black shales: insights from the Upper Devonian New Albany Shale, Illinois Basin. Int J Coal Geol 217:103351. https://doi.org/10.1016/j.coal.2019.103351

Lüning S, Kolonic S (2003) Uranium spectral gamma-ray response as a proxy for organic richness in black shales: applicability and limitations. J Petrol Geol 26(2):153–174. https://archives.datapages.com/data/jpg/2003/02apr/0153/0153.html

Ma X, Liu B, Brazell C, Mastalerz M, Drobniak A, Schimmelmann A (2021) Methane generation from low-maturity coals and shale source rocks at low temperatures (80–120 °C) over 14–38 months. Org Geochem 155:104224. https://doi.org/10.1016/j.orggeochem.2021.104224

Martins Z, Pasek MA (2024) Delivery of organic matter to the early Earth. Elements 20:19–23. https://doi.org/10.2138/gselements.20.1.19

McDiarmid MA (2001) Depleted uranium and public health. Fifty years' study of occupational exposure provides little evidence of cancer. BMJ (Clin Res Ed) 322:123–124. https://doi.org/10.1136/bmj.322.7279.123

Meredith W, Kelland S-J, Jones DM (2000) Influence of biodegradation on crude oil acidity and carboxylic acid composition.

Org Geochem 31:1059–1073. https://doi.org/10.1016/S0146-6380(00)00136-4

Mozumder A (1999) Fundamentals of radiation chemistry. Academic Press, San Diego

Murae T, Shimokawa S, Aihara A (1996) Pyrolytic and spectroscopic studies of the diagenetic alteration of resinites. ACS Symp Ser 617:76–91. https://doi.org/10.1021/bk-1995-0617.ch004

Naumenko-Dèzes M, Kloppmann W, Blessing M, Mayer B (2022) Natural gas of radiolytic origin: an overlooked component of shale gas. PNAS 119(15):e2114720119. https://doi.org/10.1073/pnas.2114720119

Orem WH, Hatcher PG, Spiker EC, Szeverenyi NM, Maciel GE (1986) Dissolved organic matter in anoxic pore water from Mangrove Lake, Bermuda. Geochim Cosmochim Acta 50:609–618. https://doi.org/10.1016/0016-7037(86)90109-2

Ravin A, Rouchon V, Blanchet D (2017) Determination of organic degradation rates in 100 My old sediments: application to Cretaceous black shale intervals from Demerara Rise, ODP Leg 207. Org Geochem 113:128–140. https://doi.org/10.1016/j.orggeochem.2017.07.019

Regulla DF, Deffner U (1982) Dosimetry by ESR spectroscopy of alanine. Int J Appl Radiat Isot 33:1101–1114. https://doi.org/10.1016/0020-708X(82)90238-1

Saito H, Suzuki N (2007) Distributions and sources of hopanes, hopanoic acids and hopanols in Miocene to recent sediments from ODP Leg 190, Nankai Trough. Org Geochem 38:1715–1728. https://doi.org/10.1016/j.orggeochem.2007.05.012

Sauvage JF, Flinders A, Spivack AJ, Pockalny R, Dunlea AG, Anderson CH, Smith DC, Murray RW, D'Hondt S (2021) The contribution of water radiolysis to marine sedimentary life. Nat Commun 12(1):1297. https://doi.org/10.1038/s41467-021-21218-z

Schimmelmann A, Qi H, Coplen TB, Brand WA, Fong J, Meier-Augenstein W, Kemp HF, Toman B, Ackermann A, Assonov S, Aerts-Bijma AT, Brejcha R, Chikaraishi Y, Darwish T, Elsner M, Gehre M, Geilmann H, Gröning M, Hélie JF, Herrero-Martín S, Meijer HAJ, Sauer PE, Sessions AL, Werner RA (2016) New organic reference materials for hydrogen, carbon, and nitrogen stable isotope-ratio measurements: caffeines, *n*-alkanes, fatty acid methyl esters, glycines, L-valines, polyethylenes, and oils. Anal Chem 88:4294–4302. https://doi.org/10.1021/acs.analchem.5b04392

Schmoker JW (1981) Determination of organic-matter content of Appalachian Devonian shales from gamma-ray logs. Am Assoc Pet Geol Bull 65:1285–1298. https://doi.org/10.1306/03B5949A-16D1-11D7-8645000102C1865D

Schulz HM, Yang S, Schovsbo NH, Rybacki E, Ghanizadeh A, Bernard S, Mahlstedt N, Krüger M, Amann-Hildebrandt A, Krooss BM, Meier T, Reinick A (2021) The Furongian to Lower Ordovician Alum Shale Formation in conventional and unconventional petroleum systems in the Baltic Basin—a review. Earth Sci Rev 218:103674. https://doi.org/10.1016/j.earscirev.2021.103674

Shostenko AG, Olejniczak A, Truszkowski S (2006) Effects of tritium β-radiation and cobalt γ-radiation on vacuum oils. High Energy Chem 40:146–148. https://doi.org/10.1134/S0018143906030039

Silva RC, Snowdon LR, Huang H, Nightingale M, Becker V, Taylor S, Mayer B, Pedersen JH, di Primio R, Larter S (2019) Radiolysis as a source of ^{13}C depleted natural gases in the geosphere. Org Geochem 138:103911. https://doi.org/10.1016/j.orggeochem.2019.103911

Swallow AJ (1960) Radiation chemistry of organic compounds. International series of monographs on radiation effects in materials, vol 2. Oxford, Pergamon Press. Available as Google book. https://books.google.com/books?hl=en&lr=&id=rCv-BAAAQBAJ&oi=fnd&pg=PP1&dq=Radiation+Chemistry+of+Organic+Compounds.+Pergamon+Press&ots=_HCGZFL_zE&sig=sxZ67GaYy611AhY2np_3LFp_puY#v=onepage&q=Radiation%20Chemistry%20of%20Organic%20Compounds.%20Pergamon%20Press&f=false

Vandegrift GF, Winans RE, Scott RG, Horwitz EP (1980) Quantitative study of the carboxylic acids in Green River oil shale bitumen. Fuel 59:627–633. https://doi.org/10.1016/0016-2361(80)90124-6

VanEngelen MR, Szilagyi RK, Gerlach R, Lee BD, Apel WA, Peyton BM (2011) Uranium exerts acute toxicity by binding to pyrroloquinoline quinone cofactor. Environ Sci Technol 45:937–942. https://doi.org/10.1021/es101754x

Voevodskii VV, Molin YN (1962) On the radiation stability of solid organic compounds. Radiat Res 17:366–378. https://doi.org/10.2307/3571099

Wang W, Liu C, Liu W, Wang X, Guo P, Wang J, Wang Z, Li Z, Zhang D (2022) Dominant products and reactions during organic matter radiolysis: implications for hydrocarbon generation of uranium-rich shales. Mar Pet Geol 137:105497. https://doi.org/10.1016/j.marpetgeo.2021.105497

Yang S, Schulz HM, Horsfield B, Schovsbo NH, Grice K, Zhang J (2020) Geological alteration of organic macromolecules by irradiation: implication for organic matter occurrence on Mars. Geology 48:713–717. https://doi.org/10.1130/G47171.1

Yang S, Schulz HM, Horsfield B, Schovsbo NH, Noah M, Panova E, Rothe H, Hahne K (2018) On the changing petroleum generation properties of Alum Shale over geological time caused by uranium irradiation. Geochim Cosmochim Acta 229:20–35. https://doi.org/10.1016/j.gca.2018.02.049

Yang S, Schulz HM, Schovsbo N, Mayanna S (2019) The organic geochemistry of "Kolm", a unique analogue for the understanding of molecular changes after significant uranium irradiation. Int J Coal Geol 209:89–93. https://doi.org/10.1016/j.coal.2019.05.004

Yin M, Snowdon LR, Silva RC, Huang H, Larter S (2023) Impacts of natural irradiation on sedimentary organic matter – a review. Org Geochem 180:104602. https://doi.org/10.1016/j.orggeochem.2023.104602